The Astrophysical Journal Letters, 941:L35 (5pp), 2022 December 20 https://doi.org/10.3847/2041-8213/aca671

Can 1D Radiative-equilibrium Models of Faculae Be Used for Calculating Contamination of Transmission Spectra?

Veronika Witzke[1], Alexander I. Shapiro[1], Nadiia M. Kostogryz[1], Robert Cameron[1], Benjamin V. Rackham[2,3,6], Sara Seager[2,3,4], Sami K. Solanki[1], and Yvonne C. Unruh[5]
[1] Max Planck Institute for Solar System Research, Justus-von-Liebig-Weg 3, D-37077 Göttingen, Germany; witzke@mps.mpg.de
[2] Department of Physics and Kavli Institute for Astrophysics and Space Research, Massachusetts Institute of Technology, Cambridge, MA 02139, USA
[3] Department of Earth, Atmospheric and Planetary Sciences, Massachusetts Institute of Technology, Cambridge, MA 02139, USA
[4] Department of Aeronautics and Astronautics, Massachusetts Institute of Technology, 77 Massachusetts Avenue, Cambridge, MA 02139, USA
[5] Blackett Laboratory, Imperial College London, South Kensington Campus, London SW7 2AZ, UK
Received 2022 October 20; revised 2022 November 21; accepted 2022 November 28; published 2022 December 22

Abstract

The reliable characterization of planetary atmospheres with transmission spectroscopy requires realistic modeling of stellar magnetic features, since features that are attributable to an exoplanet atmosphere could instead stem from the host star's magnetic activity. Current retrieval algorithms for analyzing transmission spectra rely on intensity contrasts of magnetic features from 1D radiative–convective models. However, magnetic features, especially faculae, are not fully captured by such simplified models. Here we investigate how well such 1D models can reproduce 3D facular contrasts, taking a G2V star as an example. We employ the well-established radiative magnetohydrodynamic code MURaM to obtain three-dimensional simulations of the magnetoconvection and photosphere harboring a local small-scale dynamo. Simulations without additional vertical magnetic fields are taken to describe the quiet solar regions, while simulations with initially 100 G, 200 G, and 300 G vertical magnetic fields are used to represent facular regions of different magnetic flux density. Subsequently, the spectra emergent from the MURaM cubes are calculated with the MPS-ATLAS radiative transfer code. We find that the wavelength dependence of facular contrast from 1D radiative–convective models cannot reproduce facular contrasts obtained from 3D modeling. This has far-reaching consequences for exoplanet characterization using transmission spectroscopy, where accurate knowledge of the host star is essential for unbiased inferences of the planetary atmospheric properties.

Unified Astronomy Thesaurus concepts: Radiative magnetohydrodynamics (2009); Solar physics (1476); Solar active regions (1974); Solar faculae (1494); Exoplanet atmospheric composition (2021); Exoplanet atmospheres (487)

1. Introduction

In the past decade the transit method has become a highly productive tool for exoplanet hunting and characterization. During a transit, exoplanets appear larger at wavelengths where their atmosphere absorbs or scatters the radiation emitted by the host star. This allows identifying the composition of the planetary atmosphere by measuring a wavelength-dependent exoplanetary radius (a so-called transmission spectrum; Seager & Sasselov 2000; Brown 2001; Charbonneau et al. 2002). Transmission spectroscopy was given a huge boost by the advent of the James Webb Space Telescope (JWST), which has already been used to make the first definitive detection of carbon dioxide in an exoplanet atmosphere (The JWST Transiting Exoplanet Community Early Release Science Team et al. 2022) and even holds the promise of studying atmospheres of rocky exoplanets (e.g., Barstow & Irwin 2016; Morley et al. 2017; Lustig-Yaeger et al. 2019).

Apart from planetary atmospheres, signals in transmission spectra may result from surface inhomogeneities of host stars, caused by their magnetic activity. Namely, magnetic features that remain unocculted during the transit induce a wavelength-dependent offset that affects the relative depth of transits and, consequently, the deduced planetary radii (see, e.g., Rackham et al. 2018, 2019, and references therein). For example, dark magnetic features outside of the transit chord lead the stellar disk to be darker on average than it is within the transit chord. This leads to increased relative transit depth and inferred planetary radii, which can be misinterpreted as absorption or scattering in the exoplanetary atmosphere. Similarly, unocculted bright features decrease transit depths and thus can mask the genuine signal from the exoplanetary atmosphere. In many cases the signal from stellar magnetic activity can significantly complicate the interpretation of transmission spectra (see, e.g., the report from the NASA Exoplanet Exploration Program Analysis Group Study Analysis Group 21 for a detailed review; Rackham et al. 2022). Recent examples include Barclay et al. (2021), who showed that the recently discovered water vapor signal on the habitable-zone sub-Neptune exoplanet K2-18b (Benneke et al. 2019) can be equally well explained by the magnetic activity of the host star. Similarly, the analysis of WASP-103b's transmission spectrum by Kirk et al. (2021) revealed strong evidence for magnetic activity of the host star (4.3σ) and only weak evidence for absorption from the planetary atmosphere (with signals from H_2O, HCN, and TiO suggested at 1.9σ, 1.7σ, and 2.1σ, respectively).

The algorithms used to extract information from transmission spectra rely on the differences between the wavelength

[6] 51 Pegasi b Fellow.

dependence of the planetary signal and of the activity contamination in order to disentangle them. Until now, calculations of the wavelength-dependent activity contamination, which is an input of the retrieval algorithms, have represented spectra of magnetic features by radiative-equilibrium spectra of quiet stars with different effective temperatures (Husser et al. 2013). Specifically, spots and faculae have been approximated by cooler and hotter stellar atmospheres, respectively (see the detailed discussion in Rackham et al. 2022). One can expect that such approximations introduce significant inaccuracies. In particular, faculae are formed by small-scale magnetic concentrations (Solanki et al. 2006) and are heated by hot walls surrounding them (see, e.g., Figure 5 and its detailed discussion in the review by Solanki et al. 2013). Thus, their brightness contrast is defined by 3D effects, which cannot be properly represented in one-dimensional (1D) radiative-equilibrium (RE) models.

Since accurate knowledge of the activity contamination and, in particular, its wavelength dependence is essential for advancing exoplanet characterization, we examine the accuracy of 1D-approximated facular contrasts by comparing them to facular contrasts from three-dimensional (3D) radiative magnetohydrodynamic (MHD) simulations with the MURaM code (Vogler et al. 2005; Rempel 2014, 2016). Simulations of the solar atmosphere with the MURaM code have reached a high level of realism, reproducing highly detailed solar observations. They have been used to treat the emergence of solar surface magnetic flux (Rempel & Cheung 2014; Chen et al. 2017), various magnetic features on the solar surface (Vogler et al. 2005; Cameron et al. 2007; Rempel et al. 2009), as well as the contribution of the convection (see Shapiro et al. 2017) and small-scale magnetic concentrations (see Yeo et al. 2017) to solar brightness variability.

In this study we focus on a star with solar fundamental parameters and model faculae by initially adding a vertical magnetic field of 100 G, 200 G, and 300 G to the state-of-the-art MURaM simulations of the small-scale dynamo (SSD) by Bhatia et al. (2022) and Witzke et al. (2022). In Section 2 we introduce the 3D approach for calculating facular contrasts and discuss the results. Subsequently, in Section 3 we compare the 3D facular contrast to 1D models, focusing on whether it is possible to reproduce 3D results. In Section 4 we give a brief summary along with a discussion of future goals.

2. 3D Modeling with the MURaM Code

The atmospheric structures for faculae and quiet regions are calculated using the "box-in-a-star" approach by employing the 3D radiative MHD code MURaM. MURaM solves the conservative MHD equations for a compressible, partially ionized plasma to model the dynamics and energy transport in a Cartesian box. The radiative transfer (RT) in the MURaM code is performed using a multigroup scheme with short characteristics (Nordlund 1982). For the equation of state, pretabulated look-up tables generated by the FreeEOS code (Irwin 2012) are employed. The simulated box covers 9 Mm × 9 Mm (512 × 512 grid points) in the horizontal direction and 5 Mm in depth with a resolution of 10 km.

Our description of the quiet Sun is based on the most up-to-date 3D simulations as presented in Bhatia et al. (2022) and Witzke et al. (2022). One novel feature of these simulations is that they account for an SSD operating near the stellar surface. The SSD leads to the formation of ubiquitous small-scale mixed polarity magnetic features that are always present at the solar surface, leading to considerable magnetic flux (Khomenko et al. 2003; Lites & Socas-Navarro 2004; Berdyugina & Fluri 2004; Bueno et al. 2004; Stenflo 2013). In our SSD simulations, the mean absolute value of the vertical magnetic field at the solar optical surface is 71 G (Witzke et al. 2022), which agrees well with solar observations (see a detailed discussion in Rempel 2014, 2020). Investigating solar facular regions, Schrijver & Harvey (1994) found that their mean magnetic flux density is about 100–150 G independent of the size of the facular region and activity level of the Sun (see also the discussion in Schrijver 2020). To cover the range of possible facular magnetic flux densities we added initially vertical, unipolar, and homogeneous magnetic fields of 100 G, 200 G, and 300 G to the setup we used for simulating quiet regions including the SSD. Our 100 G and 200 G simulations represent solar facular regions, while 300 G simulations were added to describe the cores of solar facular regions (see, e.g., Yeo et al. 2017) as well as facular regions that might be present on surfaces of stars significantly more active than the Sun. We note that in a previous study Norris (2019) showed facular contrasts for different stellar types. However, at that time SSD simulations were not yet available and, thus, the quiet regions were modeled without any magnetic fields using hydrodynamic simulations.

For the spectra emergent from the 3D cubes, we consider a spectral range of 200–2000 nm. The calculations are performed at low spectral resolution using the MPS-ATLAS code (Witzke et al. 2021), which incorporates the new setup for opacity distribution functions by Cernetic et al. (2019) into a greatly updated version of the ATLAS9 code by Kurucz (2005). The element abundance used for calculating the MURaM cubes as well as spectra emerging from the MURaM cubes are taken from Asplund et al. (2009). The spectral synthesis is performed along rays with different viewing angles, from $\mu = 1.0$ (disk center) to $\mu = 0.1$ (limb) in steps of 0.1 (where μ is the cosine of the angle between the observer's line of sight and the local stellar radius).

For each of the four setups, that is, the pure SSD setup representing the quiet Sun and the three setups with added magnetic fields representing faculae, we store a time series of 40 independent 3D cubes within a time interval of 10 solar hours. Subsequently, for each viewing angle, μ, the spectra are first averaged over all rays in each cube and then over all cubes in the time series. Then we define the relative facular contrast as

$$C_B(\lambda, \mu) = (I_B(\lambda, \mu) - I_{QS}(\lambda, \mu))/I_{QS}(\lambda, \mu), \quad (1)$$

where $I_{QS}(\lambda, \mu)$ is spectral intensity from the quiet Sun (represented by the SSD setup) and $I_B(\lambda, \mu)$ (with $B = 100$ G, 200 G, and 300 G) are from setups representing faculae.

Blue and black lines in Figure 1 show the spectral dependence of the relative facular contrasts at the disk center ($\mu = 1.0$) and limb ($\mu = 0.1$) as well as disk-integrated values. One can see that the contrasts strongly increase from the disk center to the limb. The contrasts change by several orders of magnitude from the ultraviolet (UV) to the infrared (IR), with disk-center contrasts even becoming negative at some wavelengths (blue parts of the curves shown in Figure 1), so we plot the absolute values.

With increasing magnetic flux density, the facular regions become dark at disk center, first in the IR then also in the

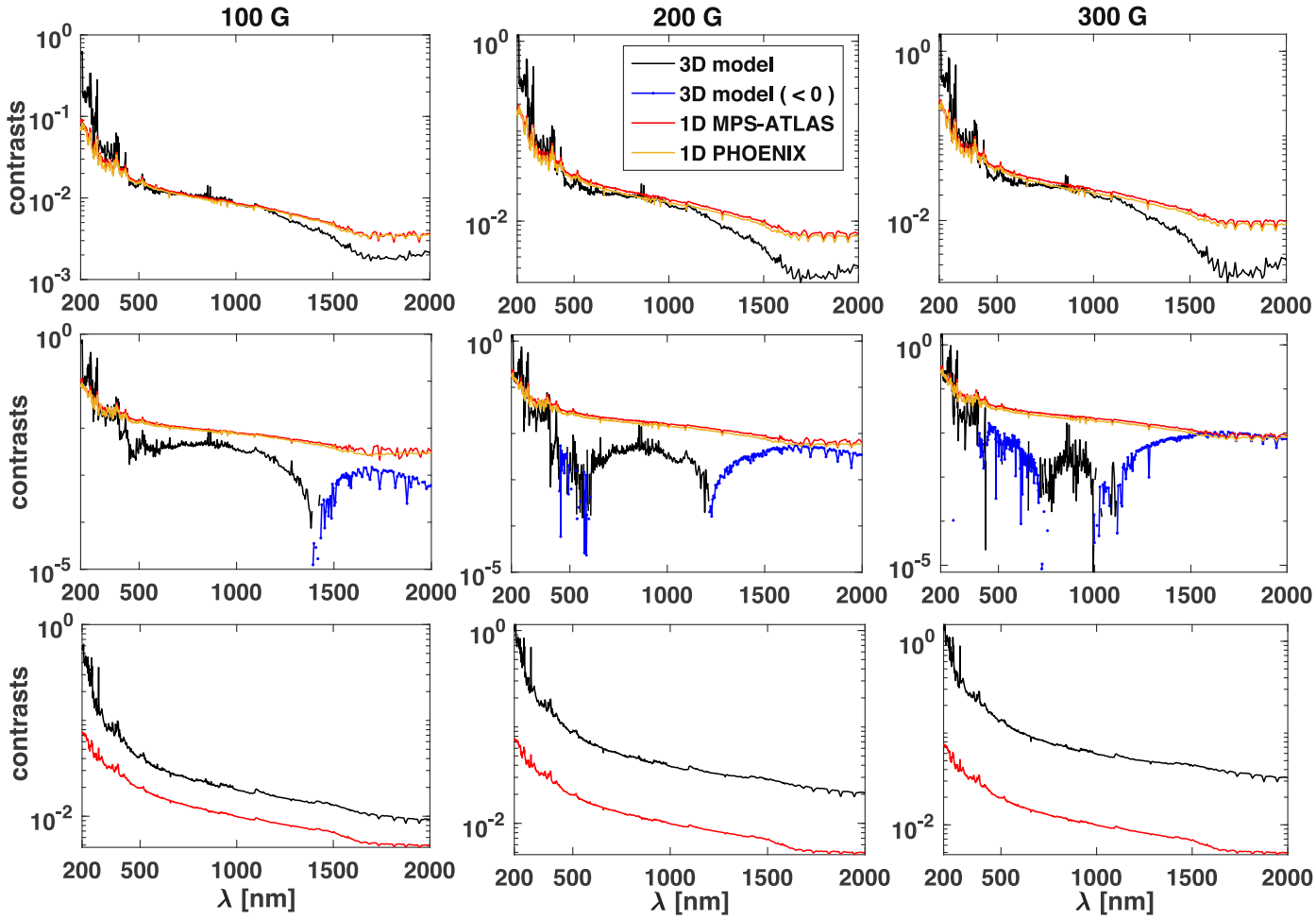

Figure 1. Relative facular contrast from 3D simulations (as given in Equation (1)) and from 1D models (as discussed in Section 3) for facular regions with different magnetic flux density values (left to right columns) and viewing angles (top to bottom rows). The top row shows the relative contrast for the disk-integrated flux, the middle row for the disk center, and the bottom row for the limb ($\mu = 0.1$).

visible (see the middle panel of Figure 1). Strikingly, the disk-integrated and disk-center contrasts show a very complex and nonmonotonous wavelength dependence. At the limb, however, the contrast does not show strongly pronounced line features and appears smoother. This is because of the effect of spectral lines (for a detailed discussion see Shapiro et al. 2015) that become progressively more important toward the disk center.

3. Comparison of Contrasts from 1D and 3D Models

To compare the facular contrasts presented in Section 2 to contrasts obtained by 1D modeling, we generate 1D atmospheric structures under the assumption of radiative–convective equilibrium with the treatment of the convection described by mixing length theory (Böhm-Vitense 1958). Subsequently, we calculate the specific intensities for the same viewing angles as used in the 3D approach. We note that the 1D calculations using the MPS-ATLAS code have been extensively validated against available observations and models of quiet solar/stellar atmospheres (see Witzke et al. 2021; Kostogryz et al. 2022). Moreover, we compare the 3D contrasts to the state-of-the-art practice in exoplanetary atmospheric retrievals, namely, contrasts derived from the PHOENIX spectral grid (Husser et al. 2013).

In our first experiment effective temperatures, $T_{\rm eff}$, of the 1D atmospheric structures are chosen so as to produce the same disk-integrated bolometric intensity outputs as those of the 3D simulations averaged over a period of ∼10 hr of solar time. These are 5787, 5805, 5823, and 5835 K for the SSD, 100 G, 200 G, and 300 G setups, respectively. Consequently, 1D atmospheres with the above effective temperatures are considered to represent faculae of different strengths of intensities. The other fundamental parameters such as the surface gravity ($\log g = 4.3$) and metallicity ($\mathrm{M/H} = 0.0$) are kept the same as in the MURaM simulations. For the contrasts derived from the PHOENIX grid,[7] we interpolated the disk-integrated flux and the specific intensities for disk center to the desired effective temperature and surface gravity from the closest available stellar parameters. We did not consider calculations for the limb, because specific intensities in the PHOENIX grid are calculated for different viewing-angle grids depending on stellar parameters, which makes interpolating even more inaccurate. The facular contrasts are then calculated employing Equation (1), using spectra emergent from the 1D models with the effective temperatures given above.

The 1D contrasts calculated this way are shown in Figure 1 (red and orange lines). It becomes evident that at disk center

[7] http://phoenix.astro.physik.uni-goettingen.de

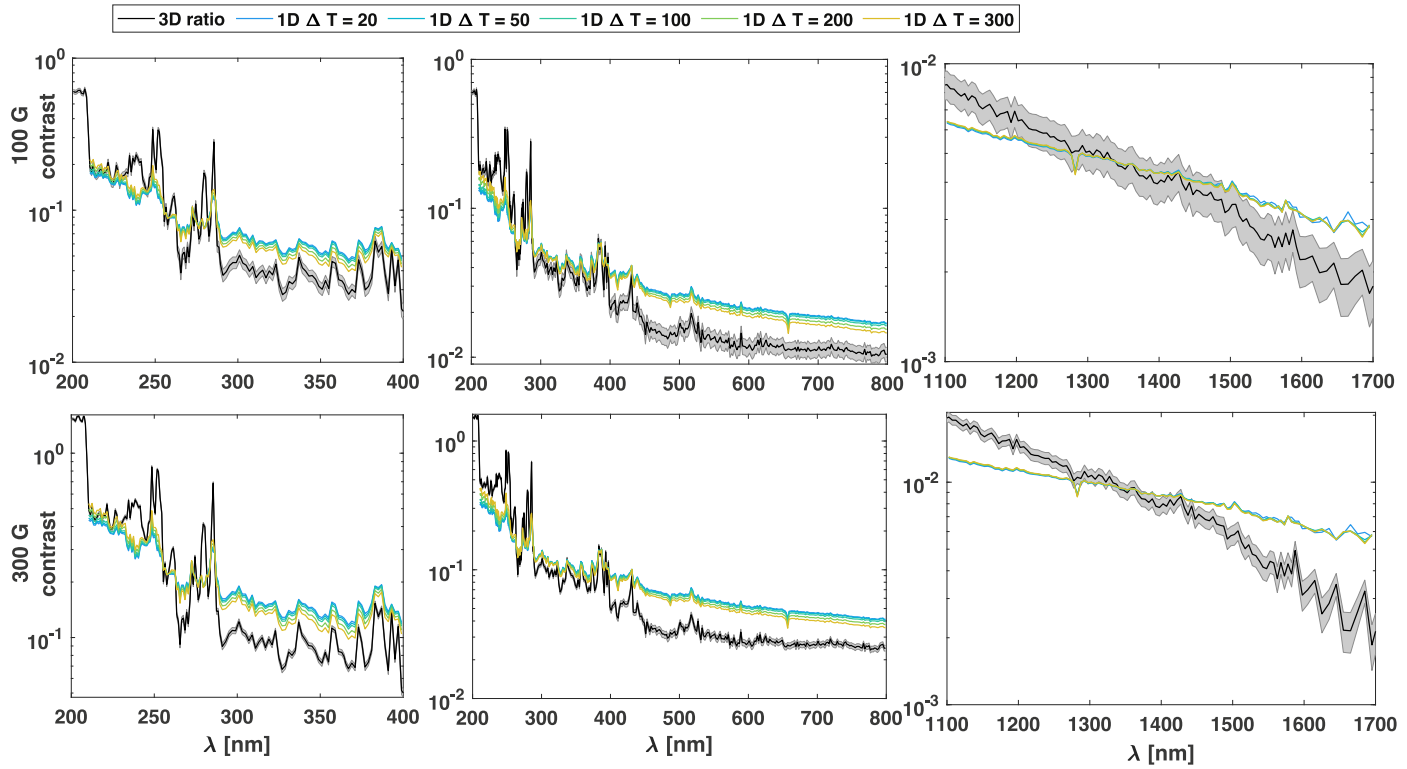

Figure 2. Disk-integrated relative facular contrast from 3D simulations (as given in Equation (1)) and normalized (see the text for details) relative contrasts from 1D models for different ΔT. The gray shaded area corresponds to the standard deviation of the scatter in contrasts due to temporal fluctuations in the 3D simulations. Different values of magnetic flux density (100 G in the top row and 300 G in the bottom row) and different wavelength intervals (left to right columns) are shown.

and integrated over the disk, the wavelength dependence of the 3D and 1D contrasts are substantially different: In particular, 1D modeling greatly overestimates the contrast in the visible and IR, but underestimates it in the UV compared to contrast modeled in 3D (see the top and middle panels of Figure 1). This implies that the disk-center and disk-integrated facular contrasts cannot be even remotely approximated by 1D radiative-equilibrium models. There are only a few and small differences between the MPS-ATLAS contrasts and the PHOENIX contrast. Thus, at disk center, PHOENIX contrasts in the IR display fewer line features compared to MPS-ATLAS contrasts.

At the same time, the wavelength dependences of the 1D and 3D contrasts at the limb are similar (see the bottom panels of Figure 1), but 1D facular contrasts are substantially lower than contrasts given by the 3D simulations. Consequently, facular contrasts at the limb can be approximated reasonably by 1D modeling but with significantly overestimated facular temperatures (since an increase of the facular temperature will lead to a scaling of the facular contrast with a factor only slightly dependent on wavelength; see discussion of Figure 2).

This result can be understood by recalling that faculae are caused by ensembles of small-scale magnetic concentrations. These concentrations can be well represented by flux tubes (see reviews by Solanki et al. 2006, 2013). The temperature structure within these flux tubes is strongly affected by the radiative heating from the hot walls and, thus, cannot be approximated by a radiative–convective equilibrium 1D model. Consequently, these models dramatically fail to describe the wavelength dependence of facular contrast at the disk center and intermediate disk positions. The emergent intensity of faculae at the limb comes from the hot walls themselves, which can be reasonably approximated by 1D radiative–convective models.

The retrieval algorithms used for the analysis of transmission spectra usually keep the surface coverage fraction of stellar magnetic features as a free parameter that is constrained during the fitting of the transmission spectra (see, e.g., a detailed discussion in Kirk et al. 2021). Therefore only the wavelength dependence of the facular contrast is important for disentangling between planetary and facular signatures in transmission spectra—any relative offset in facular contrast can be compensated by scaling the surface coverage fraction of faculae without affecting the retrieved planetary signal.

In this context, we conduct our second experiment to investigate whether 1D models with arbitrary chosen temperatures (in contrast to the first experiment shown in Figure 1, where we took temperatures from the 3D simulations) can reproduce the wavelength dependence of facular contrast in spectral intervals that are often used in transmission spectroscopy (see, e.g., Wakeford et al. 2020; Lothringer et al. 2022), namely, 200–400 nm, 200–800 nm, and 1100–1700 nm. For this we represent the quiet Sun by the 1D model with effective temperature $T_{\rm QS} = 5790\,K$ and faculae by 1D models with temperatures $T_{\rm QS} + \Delta T$, where we consider $\Delta T = 20$, 50, 100, 200, and 300 K. We note that the exact choice of T_{QS} plays little role in our experiment since the intensity contrasts mainly depend on ΔT.

In each of the three wavelength intervals, we normalize the 1D contrast, so that the integrals of 1D and 3D contrasts over the corresponding wavelength interval are equal. The result is presented in Figure 2, which shows the normalized 1D disk-integrated contrasts for different ΔT values and corresponding 3D contrasts for different magnetizations. The contrast below

210 nm has a steep increase due to the Al I ionization edge. Thus, we excluded the region 200 to 210 nm from normalization and show 1D contrasts only longward of 210 nm.

Figure 2 shows that the wavelength dependence of the 1D contrasts is only barely affected by the value of ΔT. In particular, they share all spectral features in the UV and in the visible. 1D RE models result in a totally different overall slope compared to the 3D contrast even in the relatively narrow spectral intervals shown in Figure 2. We note that the overall slope is mainly determined by the behavior of the contrast in continuum. Furthermore, one can see that 1D calculations dramatically fail to capture the sophisticated wavelength dependence of facular contrast caused by spectral lines and revealed by the 3D calculations. The more pronounced lines in the 3D contrasts can be attributed to different vertical temperature gradients in the photosphere and to the temperature inhomogeneities due to granulation and magnetic fields.

4. Implications and Future Goals

We showed that facular contrast calculated using 1D models fail to reproduce the complex wavelength dependence that is found using 3D models. Furthermore, contrasts from 1D radiative-equilibrium models cannot be fudged by adjusting the fraction of faculae present on the surface to get a closer match with contrasts from 3D models.

This result has consequences for transmission spectroscopy of transiting exoplanets, which is a widely used technique to deduce information on the structure and composition of exoplanet atmospheres. Conclusions drawn from transmission spectroscopy of transiting exoplanets, in particular, those relying on UV and blue optical data of planets transiting active stars, are potentially inaccurate, as the transmission spectra may be compromised by inhomogeneities on the host star, which so far were modeled with 1D radiative-equilibrium models (Espinoza et al. 2018; Kirk et al. 2021; Welbanks & Madhusudhan 2022).

In this work we focused on the solar case to analyze if contrasts from 1D radiative-equilibrium models can reproduce contrasts from 3D MHD simulations. Since we find that it is essential to use 3D models for active region modeling, in forthcoming publications we will extend our calculations of 3D facular contrasts from the solar fundamental parameters to other main-sequence stars of different metallicity and spectral type using the simulations of Bhatia et al. (2022) and Witzke et al. (2022). We plan to complement this work by computing spot contrasts using simulations by Panja et al. (2020).

We would like to thank the anonymous referee for helpful comments. This work has received funding from the European Research Council (ERC) under the European Union's Horizon 2020 research and innovation program (grant agreement No. 715947). This work has been partially supported by the Max Planck Society's grant "PLATO Science" and DLR's PLATO grant Nos. 50OO1501 and 50OP1902. This work was supported by the Science and Technology Facilities Council [ST/S000372/1 and ST/W000989/1]. B.V.R. thanks the Heising-Simons Foundation for support.

ORCID iDs

Veronika Witzke https://orcid.org/0000-0002-0929-1612
Alexander I. Shapiro https://orcid.org/0000-0002-8842-5403
Nadiia M. Kostogryz https://orcid.org/0000-0002-6087-3271
Robert Cameron https://orcid.org/0000-0001-9474-8447
Benjamin V. Rackham https://orcid.org/0000-0002-3627-1676
Sami K. Solanki https://orcid.org/0000-0002-3418-8449
Yvonne C. Unruh https://orcid.org/0000-0001-8217-6998

References

Asplund, M., Grevesse, N., Sauval, A. J., & Scott, P. 2009, ARA&A, 47, 481
Barclay, T., Kostov, V. B., Colon, K. D., et al. 2021, AJ, 162, 300
Barstow, J. K., & Irwin, P. G. J. 2016, MNRAS, 461, L92
Benneke, B., Wong, I., Piaulet, C., et al. 2019, ApJL, 887, L14
Berdyugina, S. V., & Fluri, D. M. 2004, A&A, 417, 775
Bhatia, T. S., Cameron, R. H., Solanki, S. K., et al. 2022, A&A, 663, A166
Böhm-Vitense, E. 1958, ZAp, 46, 108
Brown, T. M. 2001, ApJ, 553, 1006
Bueno, J. T., Shchukina, N., & Ramos, A. A. 2004, Natur, 430, 326
Cameron, R., Schussler, M., Vogler, A., & Zakharov, V. 2007, A&A, 474, 261
Cernetic, M., Shapiro, A. I., Witzke, V., et al. 2019, A&A, 627, A157
Charbonneau, D., Brown, T. M., Noyes, R. W., & Gilliland, R. L. 2002, ApJ, 568, 377
Chen, F., Rempel, M., & Fan, Y. 2017, ApJ, 846, 149
Espinoza, N., Rackham, B. V., Jordán, A., et al. 2018, MNRAS, 482, 2065
Husser, T. O., Wende-von Berg, S., Dreizler, S., et al. 2013, A&A, 553, A6
Irwin, A. W. 2012, FreeEOS: Equation of State for stellar interiors calculations, Astrophysics Source Code Library, ascl:1211.002
Khomenko, E. V., Collados, M., Solanki, S. K., Lagg, A., & Trujillo Bueno, J. 2003, A&A, 408, 1115
Kirk, J., Rackham, B. V., MacDonald, R. J., et al. 2021, AJ, 162, 34
Kostogryz, N. M., Witzke, V., Shapiro, A. I., et al. 2022, A&A, 666, A60
Kurucz, R. L. 2005, MSAIS, 8, 14
Lites, B. W., & Socas-Navarro, H. 2004, ApJ, 613, 600
Lothringer, J. D., Sing, D. K., Rustamkulov, Z., et al. 2022, Natur, 604, 49
Lustig-Yaeger, J., Meadows, V. S., & Lincowski, A. P. 2019, AJ, 158, 27
Morley, C. V., Kreidberg, L., Rustamkulov, Z., Robinson, T., & Fortney, J. J. 2017, ApJ, 850, 121
Nordlund, A. 1982, A&A, 107, 1
Norris, C. 2019, PhD thesis, Imperial College London doi:10.25560/66259
Panja, M., Cameron, R., & Solanki, S. K. 2020, ApJ, 893, 113
Rackham, B. V., Apai, D., & Giampapa, M. S. 2018, ApJ, 853, 122
Rackham, B. V., Apai, D., & Giampapa, M. S. 2019, AJ, 157, 96
Rackham, B. V., Espinoza, N., Berdyugina, S. V., et al. 2022, arXiv:2201.09905
Rempel, M. 2014, ApJ, 789, 132
Rempel, M. 2016, ApJ, 834, 10
Rempel, M. 2020, ApJ, 894, 140
Rempel, M., & Cheung, M. C. M. 2014, ApJ, 785, 90
Rempel, M., Schussler, M., & Knolker, M. 2009, ApJ, 691, 640
Schrijver, C. J. 2020, ApJ, 890, 121
Schrijver, C. J., & Harvey, K. L. 1994, SoPh, 150, 1
Seager, S., & Sasselov, D. D. 2000, ApJ, 537, 916
Shapiro, A. I., Solanki, S. K., Krivova, N. A., et al. 2017, NatAs, 1, 612
Shapiro, A. I., Solanki, S. K., Krivova, N. A., Tagirov, R. V., & Schmutz, W. K. 2015, A&A, 581, A116
Solanki, S. K., Inhester, B., & Schussler, M. 2006, RPPh, 69, 563
Solanki, S. K., Krivova, N. A., & Haigh, J. D. 2013, ARA&A, 51, 311
Stenflo, J. O. 2013, A&ARv, 21, 66
The JWST Transiting Exoplanet Community Early Release Science Team, Ahrer, E.-M., Alderson, L., et al. 2022, arXiv:2208.11692
Vogler, A., Shelyag, S., Schussler, M., et al. 2005, A&A, 429, 335
Wakeford, H. R., Sing, D. K., Stevenson, K. B., et al. 2020, AJ, 159, 204
Welbanks, L., & Madhusudhan, N. 2022, ApJ, 933, 79
Witzke, V., Duehnen, H. B., Shapiro, A., et al. 2022, A&A, submitted, arXiv:2211.02722
Witzke, V., Shapiro, A. I., Cernetic, M., et al. 2021, A&A, 653, A65
Yeo, K. L., Solanki, S. K., Norris, C. M., et al. 2017, PhRvL, 119, 9.1102
Yeo, K. L., Solanki, S. K., Norris, C. M., et al. 2017, PhRv, 119, 091102